JMEPEG
https://doi.org/10.1007/s11665-019-04252-3

1059-9495/$19.00

On the Effect of Quenching on Postweld Heat Treatment of Friction-Stir-Welded Aluminum 7075 Alloy

S.V. Sajadifar, G. Moeini, E. Scharifi, C. Lauhoff, S. Böhm, and T. Niendorf

(Submitted February 8, 2019; in revised form July 19, 2019)

This work focuses on the effect of postweld heat treatment (PWHT) on the mechanical properties and microstructural evolution of aluminum 7075 alloy processed via friction stir welding (FSW). FSW is known to be capable of grain refinement in the nugget zone (NZ). Two different quench media (water and air) were employed for PWHT. Regardless of the quench media, the PWHT led to the occurrence of grain growth in the NZ of the FSWed aluminum 7075 alloy. Abnormal grain growth occurred in the water quenched specimen. It is shown that ductility and strength of FSWed aluminum 7075 alloy are strongly dependent on the quenching rate. Changes in the mechanical properties and microstructure reveal that only at lower cooling rate this alloy is prone to the formation of precipitate-free zones (PFZs) in the vicinity of grain boundaries. Eventually, the PFZs deteriorate mechanical properties of this alloy.

Keywords aluminum 7075, friction stir welding, mechanical properties, microstructure, postweld heat treatment

1. Introduction

Over the last decades, growing demand for utilizing lightweight materials along with the necessity of manufacturing parts being able to meet the strength requirements of recent standards motivated researchers to focus on aluminum alloys. Among aluminum alloys, aluminum 7075 (AlZnMg Cu 1.5) has been extensively utilized in aerospace, automobile, and transportation applications due to its outstanding specific strength, corrosion resistance, fatigue properties, and fracture toughness (Ref 1-4). Tensile properties of aluminum 7075 were significantly improved by equal-channel angular pressing (Ref 1). Li and Starink studied compositional variations on the characteristics of coarse intermetallic particles in 7000 series aluminum alloys (Ref 2). Accordingly, the best solution heat treatment temperature was found to be 480 °C for aluminum 7075. Solution heat treatment of this alloy at temperatures above 480 °C caused formation of detrimental intermetallic particles. Texture and microstructural evolutions of aluminum 7075 alloy during cryorolling were also investigated comprehensively showing fragmentation of grains with the rise in deformation strain (Ref 3). Elevated temperature deformation behavior and microstructural evolution of cold-rolled aluminum 7075 alloy were probed elsewhere (Ref 4). The strength of this alloy was enhanced by cold rolling up to 250 °C. At temperatures above 250 °C, the ductility of cold-rolled aluminum 7075 alloy was improved due to the activation of grain boundary mediated mechanisms. However, welding of this alloy through conventional fusion welding is highly challenging due to its sensitivity to weld solidification cracking as well as reduction of strength (grain growth and hardness reduction) (Ref 5, 6). To avoid solidification cracking of aluminum 7075 alloy in fusion welding methods, friction stir welding (FSW) was utilized (Ref 5). This welding technique could join this alloy with fewer weld defects. Cavaliere and Squillace also studied the mechanical properties of aluminum 7075 alloy fabricated via friction stir processing (FSP) (Ref 6). FSP could increase superplastic properties of this alloy. Particularly, FSW has shown high potential for welding aluminum 7075 with good dimensional stability of the welded structure and low density of weld defects (Ref 7-10).

FSW is a solid-state welding technique capable of inducing grain refinement via severe plastic deformation (SPD) (Ref 11-13). Grain refinement by SPD methods was used to promote excellent monotonic and cyclic behaviors of aluminum alloys (Ref 14-16). The postweld heat treatment (PWHT) of FSWed aluminum 7075 has recently become the focus of investigations to improve the performance of FSW joints (Ref 5, 7, 17, 18). The effect of postweld solution treatment and artificial aging on microstructure and mechanical properties of FSWed aluminum 7075 was examined in (Ref 5). T6 heat treatment of FSWed aluminum 7075 resulted in the highest strength, while this heat treatment made the joints prone to microcracking causing premature fracture. Tensile properties of FSWed aluminum 7075 alloy were investigated elsewhere (Ref 7). The combination of solution treatment and artificial aging following standard parameters for the alloy was seen to be capable of enhancing the mechanical properties of FSWed joints although all postweld heat treated specimens yet demonstrated inferior mechanical properties compared to that of aluminum 7075-T6 alloy as the parent material. Furthermore, reaging treatment including heat treatment at 220 °C for 5 min, water quenching followed by aging at T6 condition was conducted on FSW joints of 7075 alloy leading to the improvement of strength, hardness and corrosion resistance (Ref 17). This improvement was imputed to the distribution of fine precipitates in the grain interior.

S.V. Sajadifar, C. Lauhoff, and **T. Niendorf**, Institute of Materials Engineering, University of Kassel, Mönchebergstraße 3, 34125 Kassel, Germany; **G. Moeini** and **S. Böhm**, Department for Cutting and Joining Manufacturing Processes, University of Kassel, Kurt-Wolters-Straße 3, 34125 Kassel, Germany; and **E. Scharifi**, Metal Forming Technology, University of Kassel, Kurt-Wolters-Straße 3, 34125 Kassel, Germany. Contact e-mail: sajjadifar@uni-kassel.de.

Among the previous research works, the influence of the quenching conditions on the mechanical properties, precipitation hardening, and microstructural evolution of 7000 series aluminum alloys has been only briefly addressed (Ref 19-23). Generally, the increase in cooling rate resulted in a higher level of supersaturation and, hence, precipitation hardening in subsequent aging treatment (Ref 19, 20). The cooling rate was observed to have a noticeable impact on the morphologies of introduced precipitates leading to variations in mechanical properties (Ref 21). Differential scanning calorimetry (DSC) measurements proved that the increase in cooling rate contributes to hardening after aging (Ref 22). This was ascribed to the effective preservation of solute elements in solution being then available for the following aging process. However, the 7175 alloy showed a considerable reduced quench sensitivity because of higher Zn/Mg ratio as compared to the other 7000 series aluminum alloys (Ref 23). Even at slow cooling rate, aging of 7175 alloy provides microstructure with homogeneous precipitation.

Lack of data on the effect of cooling rate in post-heat treatment of FSWed aluminum 7075 is the motivation for conducting this research work. The present study investigates the impact of using different quench media during postweld heat treatment of FSWed 7075 alloy for the very first time. Results obtained by mechanical testing including hardness and tensile tests, microstructural characterization, and fractography are presented. The achievements of the present investigation introduce new findings for the advancement of FSWed structures made from age-hardenable aluminum alloys.

2. Experimental Procedure

Rolled sheets of aluminum 7075-T6 alloy with a thickness of 1.5 mm were utilized as the parent material. The chemical composition of the as-received alloy is listed in Table 1.

Aluminum 7075-T6 sheets were friction-stir-welded perpendicular to the rolling direction using a cylindrical pin with a

Table 1 Chemical composition of aluminum 7075-T6 alloy used in this study

Element	Si	Fe	Cu	Mn	Mg	Cr	Zn	Ti	Zr	Al
Weight percent	0.10	0.11	1.49	0.03	2.38	0.20	5.57	0.03	0.04	Balance

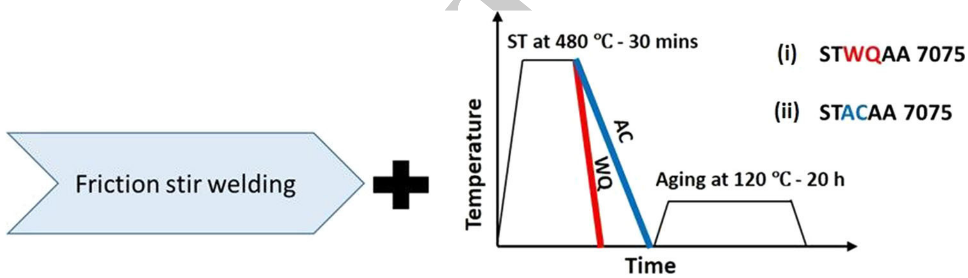

Fig. 1 Schematic detailing differences in the heat treatments applied

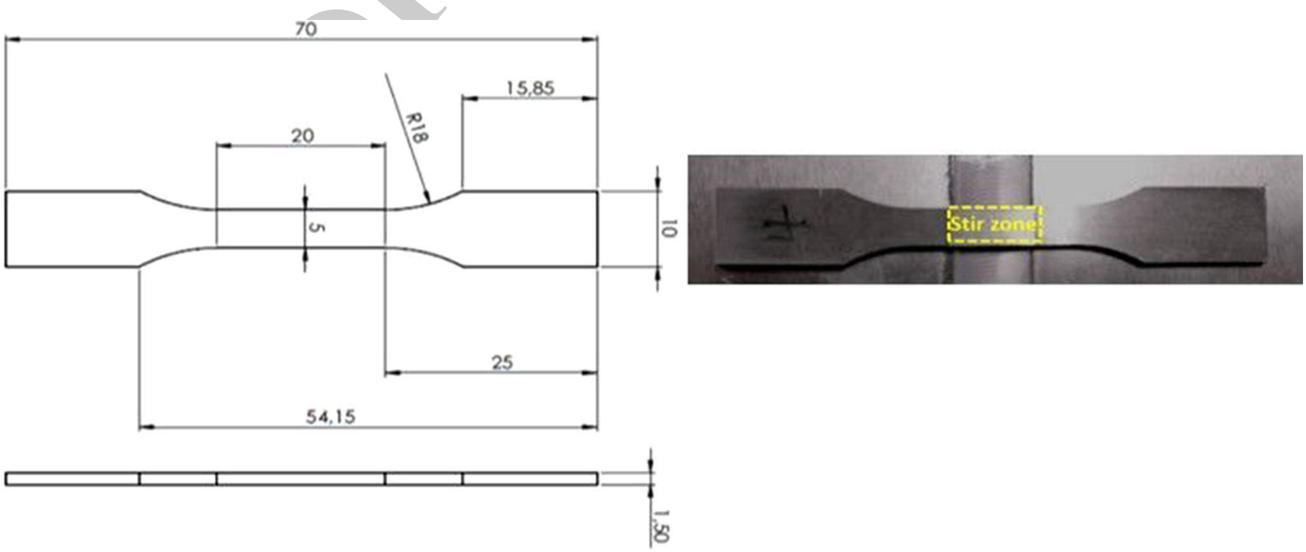

Fig. 2 Geometry of the specimen used and position of the NZ within the gage length of the specimen

Journal : JMEP_11665 Dispatch : 3-8-2019 Pages : 11
☐ LE ☐ TYPESET
Article Number : 4252 ☑ CP ☑ DISK

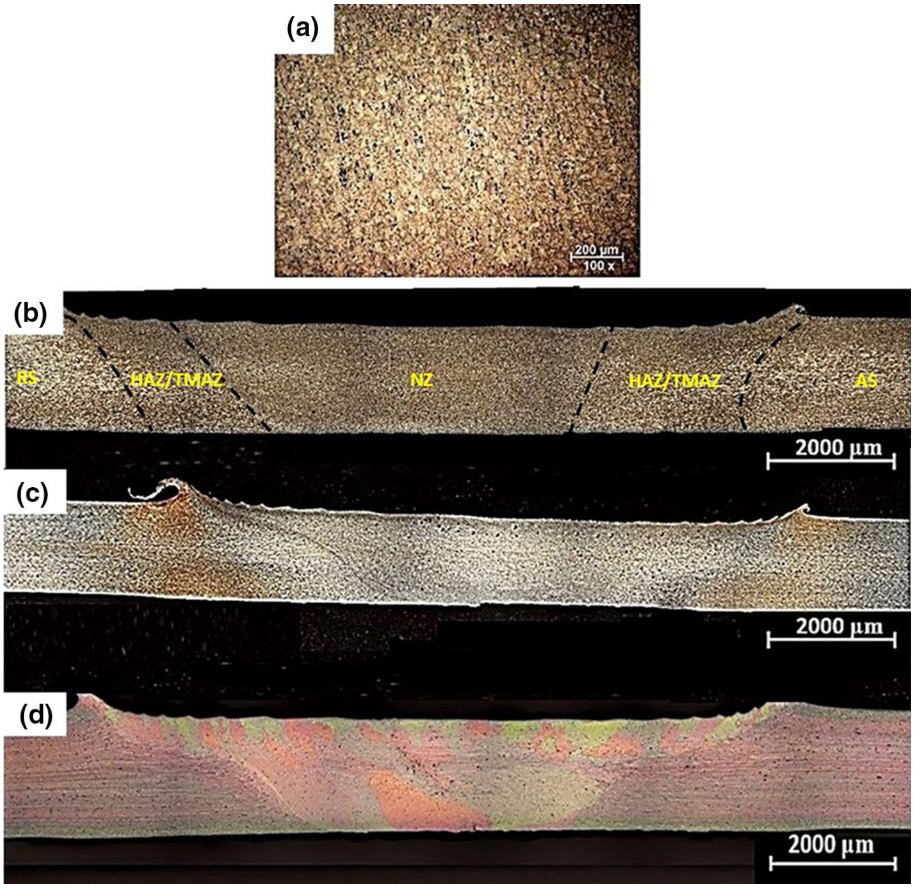

Fig. 3 Optical micrographs of (a) base metal (7075-T6 aluminum alloy), (b) FSWed, as well as PWHT (c) ST**AC**AA and (d) ST**WQ**AA aluminum 7075 alloy

diameter and length of 6 and 1.14 mm, respectively. Welding speed of 800 mm/min and tool rotational speed of 1200 rotations per minute (r/min) were applied for the FSW joints. During FSW, temperature of workpiece was measured by thermocouples. At the beginning of FSW, the temperature of sample was measured to be 20 °C. The welding was carried out in open air. The maximum temperature recorded was 430 °C. In order to evaluate the impact of PWHT, the welded joints were exposed to two different heat treatment processes, namely (1) solution treatment at 480 °C for 30 min followed by subsequent water quenching (cooling rate of 250 °C/s) and artificial aging at 120 °C for 20 h (ST**WQ**AA) and (2) solution treatment at 480 °C for 30 min followed by air cooling (cooling rate of 0.5 °C/s) and artificial aging at 120 °C for 20 h (ST**AC**AA). The schematic illustration of the heat treatment cycles is provided in Fig. 1.

Micro-Vickers hardness measurements utilizing a microhardness tester equipped with an automated stage were performed on the specimens with 100 g force and 15 s indentation duration at ambient temperature. The center-to-center distance between indents in all specimens was around 0.2 mm in X direction and 0.3 mm in Y direction. To evaluate the flow response at various conditions, room temperature tensile tests were carried out at three differing nominal crosshead speeds of 0.08 mm/min, 0.8 mm/min and 8 mm/min on flat dog-bone specimens with gage sections of 20 mm × 5 mm × 1.5 mm. Strains were measured by using an extensometer directly attached to the specimen surfaces. Specimens were electrodischarged machined (EDM) along the rolling direction and perpendicular to the welding direction as shown in Fig. 2.

Optical microscopy was utilized to characterize the evolution of the microstructure. The specimens were prepared using standard polishing procedures. Afterward, the specimens were firstly etched with a solution of 5% NaOH in H_2O and then with a Weck's reagent. A scanning electron microscope (SEM) equipped with an energy-dispersive x-ray spectroscopy (EDS) detector and an electron backscatter diffraction (EBSD) unit operating at a nominal voltage of 20 kV was used to investigate details in microstructure evolution and fracture surfaces of the specimens in various conditions. For EBSD examination, the specimens were prepared by 24 h of vibropolishing in a colloidal silica solution.

3. Results and Discussion

3.1 Microstructural Evolution

The optical micrographs of aluminum 7075 alloy in various processing states are shown in Fig. 3. Advancing side (AS), retreating side (RS), heat-affected zone (HAZ), thermomechanically affected zone (TMAZ), and nugget zone (NZ) are demonstrated in Fig. 3(b). Obviously, the microstructure of the base metal consists of coarse grains having an average grain size of 23 μm (Fig. 3a). It is very important to note that FSW

Journal : JMEP_11665 Dispatch : 3-8-2019 Pages : 11
Article Number : 4252 ☐ LE ☑ CP ☐ TYPESET ☑ DISK

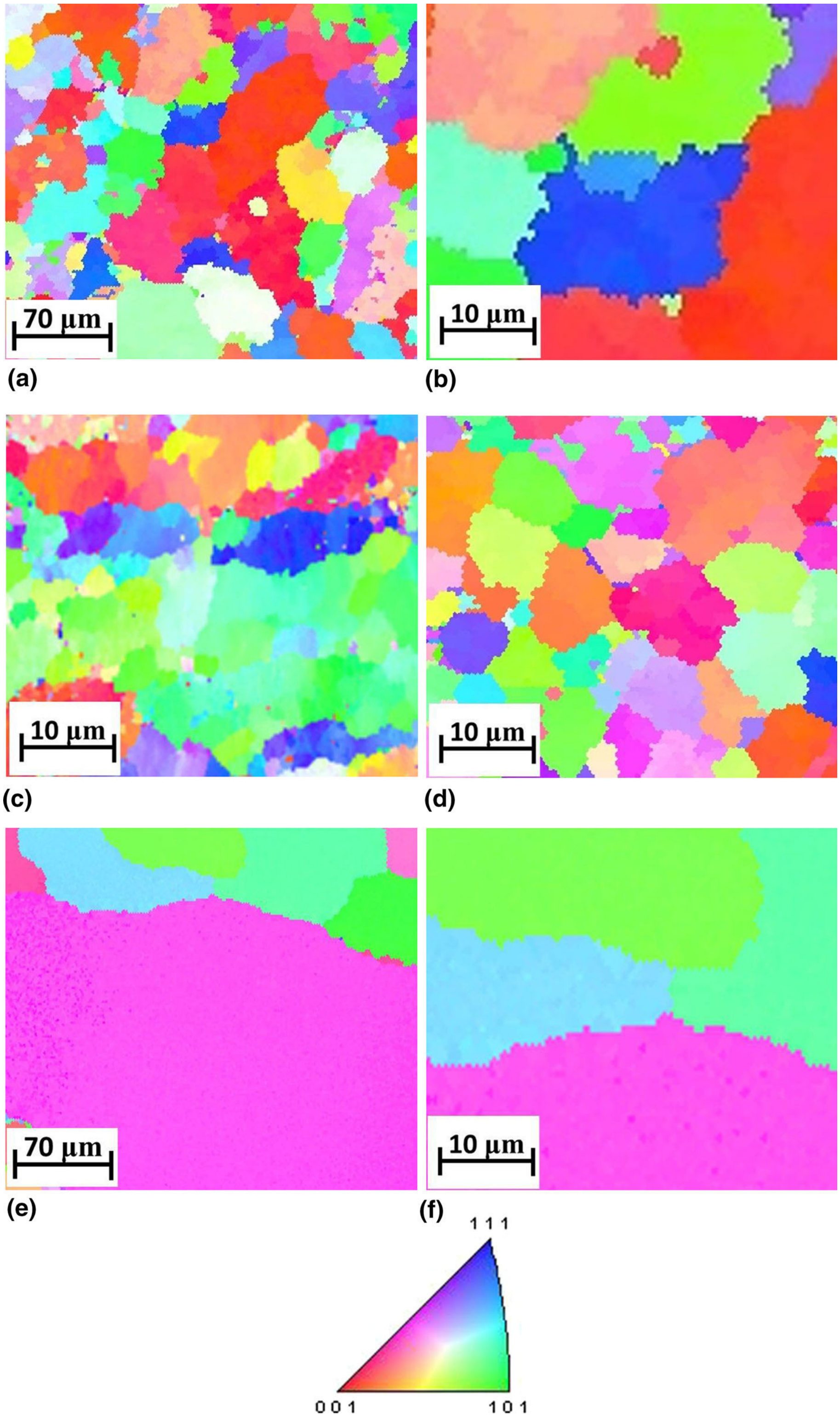

Fig. 4 EBSD images of (a) and (b) base metal (7075-T6 aluminum alloy), (c) FSWed, as well as PWHT (d) ST**AC**AA and (e), (f) ST**WQ**AA aluminum 7075 alloy. The images in (c)-(f) were captured from NZ. Color coding is according to the standard triangle shown in the bottom of the figure. See text for details

processing instigated a considerable refinement in the aluminum 7075 alloy as compared with the initial coarse microstructure (Fig. 3b). However, the microstructure of the HAZ and the base metal remain coarse-grained.

The influence of PWHT was further analyzed via EBSD. EBSD micrographs (inverse pole figure (IPF) map) of the alloy before and after FSW processing are provided in Fig. 4(b) and (c), respectively, confirming the establishment of a fine, equiaxed

Journal : JMEP_11665 Dispatch : 3-8-2019 Pages : 11
LE TYPESET
Article Number : 4252 CP DISK

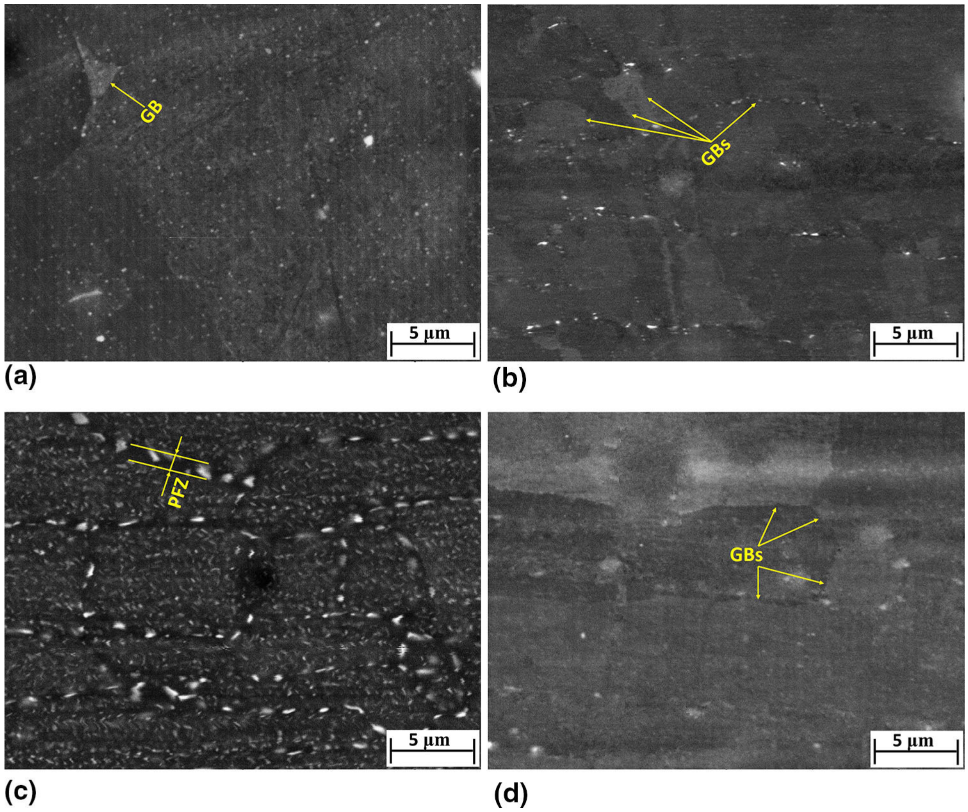

Fig. 5 SEM micrographs using BSE contrast (a) base metal (7075-T6 aluminum alloy), (b) FSWed, (c) ST**AC**AA and (d) ST**WQ**AA aluminum 7075 alloy. See text for details

grain structure with an average grain size of 2 µm in the NZ of the FSWed sample. Grain boundary misorientation distribution as deduced from EBSD analysis (not shown) revealed the efficiency of grain refinement by FSW. It is well established that FSW as an SPD processing method results in fragmentation of grains and development of refined, equiaxed grains in aluminum alloys (Ref 5-8, 24). Micrographs of the FSWed aluminum 7075 alloy followed by two different PWHTs are also represented in Fig. 4(d)–(f). It can be seen that grain growth occurred during PWHT. Interestingly, a gradual, homogeneous grain growth is evident for the ST**AC**AA specimen (Fig. 4d). Contrarily, a severe, abnormal grain growth (AGG) took place in the case of the ST**WQ**AA specimen (Fig. 4e and f). Some large and irregularly shaped grains with diameters of more than 1 mm are grown in the NZ of the ST**WQ**AA specimen. Although AGG was previously reported during PWHT included solution and natural aging treatments of FSWed aluminum 2024 alloy (Ref 25), the present investigation suggest that the AGG during PWHT can be controlled via cooling rate variations. The abnormal coarsening of the grains in the NZ can be rationalized in terms of the occurrence of static recrystallization (SRX) and the subsequent growth of newly recrystallized grains during the elevated temperature dwell time (Ref 26). For the ST**AC**AA specimen, the segregation of precipitates along the GBs upon air cooling limits the motion of high-angle grain boundaries, which is the main mechanism of grain growth (Ref 27, 28). Thus, these second phases suppress AGG in the subsequent aging treatment. The formation of precipitates along GBs will be assessed in the following section. The aging temperature and period were 120 °C (393 K) and 20 h, respectively. This temperature is about a homologous temperature of 0.5 (melting temperature of this alloy ranges from 750 to 908 K). The relatively long aging period at the homologous temperature of 0.5 resulted in severe growth of the ST**WQ**AA microstructure in the NZ. The decrease in internal energy by reducing the fraction of GBs is the related dynamic force for this severe grain growth in the NZ. Although the tendency toward rapid grain growth was already mentioned for these alloys, the impact of cooling rate on AGG was not explored in previous studies (Ref 5, 17).

SEM micrographs utilizing back-scattered electron (BSE) contrast are displayed in Fig. 5. From Fig. 5(a), it can be deduced that the base metal contains very fine and dispersed precipitates since the prior T6 heat treatment was applied to form these fine precipitates throughout the microstructure. Such fine precipitates lead to the increase in material strength as they interact with dislocations and impede their motion (Ref 29, 30). It is also noteworthy that no segregation of precipitates along the GBs was observed for the base metal. For the FSWed specimen, some large precipitates were found along the GBs although the segregation of second phase along GBs did not take place at all GBs depicted. This kind of distribution of precipitates can be attributed to the reprecipitation of (during FSW) dissolved precipitates while cooling down after FSW (Ref 30). As demonstrated in Fig. 5(c), the microstructure of the ST**AC**AA aluminum 7075 alloy consists of fine precipitates in the grain interior and some relatively coarse precipitates along the GBs. It can also be seen that a precipitate-free zone (PFZ) formed in the vicinity of the GBs in the ST**AC**AA specimen. The formation of PFZs around the GBs is expected to stem from the very low cooling rate (0.5 °C/s) after solution

Journal : JMEP_11665 Dispatch : 3-8-2019 Pages : 11
Article Number : 4252 ☐ LE ☑ CP ☐ TYPESET ☑ DISK

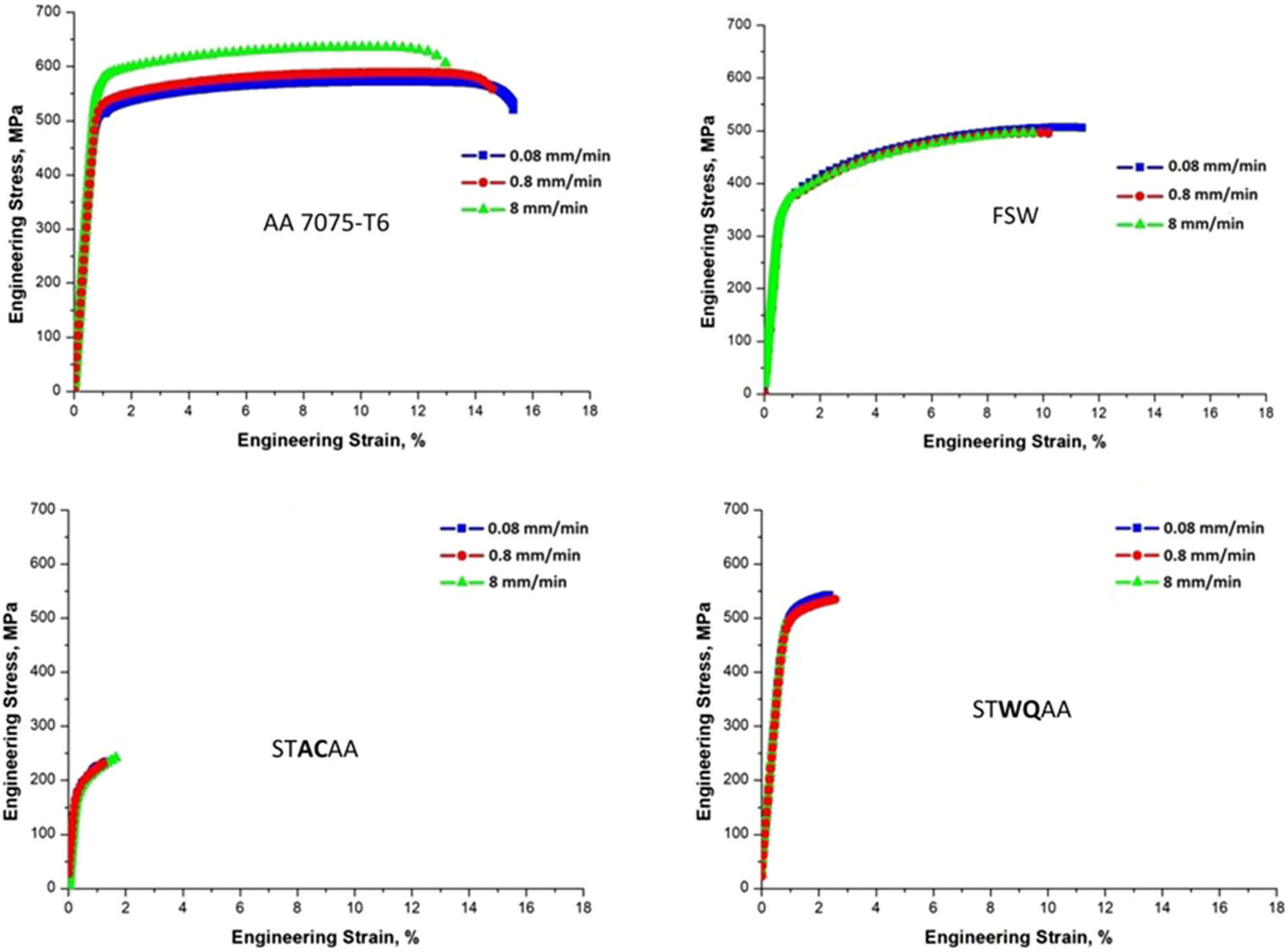

Fig. 6 Stress–strain curves of the base metal (7075-T6 aluminum alloy) and the FSWed, ST**AC**AA and ST**WQ**AA aluminum 7075 alloy conditions

Table 2 Tensile properties of aluminum 7075 alloy tested with a crosshead speed of 0.8 mm/min in different conditions

Specimen condition	Yield strength, MPa	Ultimate tensile strength, MPa	Elongation, %
Base metal	475	585	15
FSWed aluminum 7075 alloy	305	500	11
ST**AC**AA aluminum 7075 alloy	155	225	1.5
ST**WQ**AA aluminum 7075 alloy	455	555	2.5

treatment in the ST**AC**AA condition promoting the evolution of relatively large precipitates along the GBs eventually leading to a depletion of the surrounding areas in precipitate forming elements. These precipitates can grow in the subsequent aging treatment, and thus, alloying elements will further migrate from the vicinity of GBs in order to assist the growth of segregated precipitates. The presence of PFZs was reported elsewhere for a number of aluminum alloys including alloys of the 7000 series (Ref 17, 26, 29, 31-33). The effect of PFZs on the mechanical properties of aluminum 7075 alloy will be elaborated in the next section. EDS analysis was done on the segregated precipitates along the GBs of ST**AC**AA (not shown). Evidently, Mg-Zn precipitates were found on the GBs. Based on the EDS analysis results reported for 7050 and 7075 alloys, precipitates are near the stoichiometric compositions of the MgZn (η') and the $MgZn_2$ (η) phase, respectively (Ref 17, 21). On the contrary, the micrograph obtained from the STWQAA specimen (Fig. 5d) exhibits no precipitates formed alongside the GBs. Besides, the formation of PFZ is not evident for STWQAA specimen since fine and disperse precipitates throughout the microstructure (similar to the T6 state) were introduced during this PWHT. It can be deduced that the morphologies and sizes of precipitates strongly depend on the cooling rate after solution heat treatment in PWHT of 7075 alloy. The in-depth analysis of precipitate morphologies and type is currently under investigation and will be addressed in a follow-up study.

Journal : **JMEP_11665** Dispatch : **3-8-2019** Pages : **11**
Article Number : **4252**
☐ LE ☐ TYPESET
☑ CP ☑ DISK

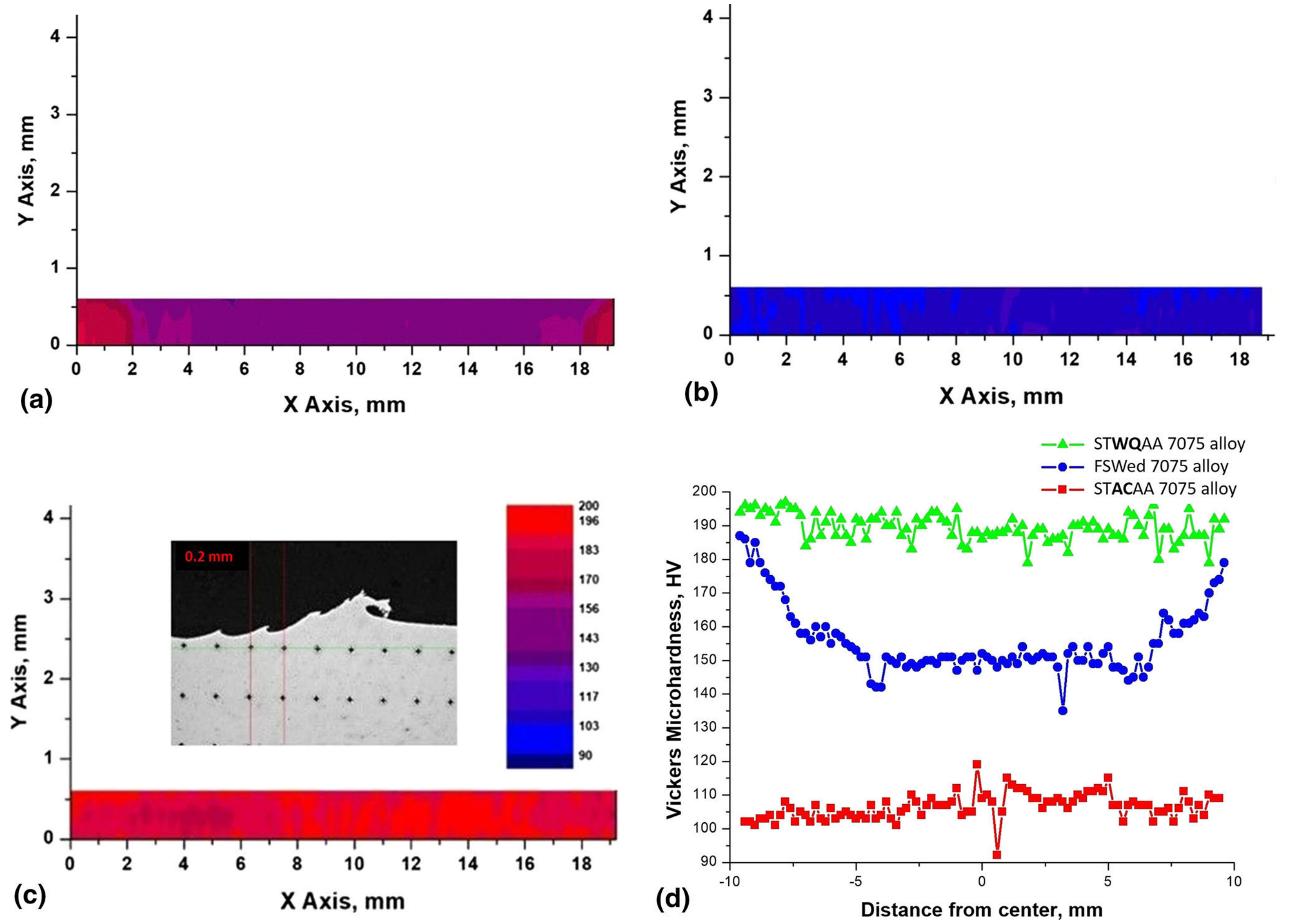

Fig. 7 Microhardness (HV 0.1) mapping of (a) FSWed, (b) ST**AC**AA and (c) ST**WQ**AA aluminum 7075 alloy over entire weld; (d) microhardness profile of aluminum 7075 alloy in different conditions. The base material revealed a homogeneous hardness of 193 ± 4 HV

3.2 Mechanical Behavior

Figure 6 shows the engineering stress–strain curves acquired from the tensile tests of aluminum 7075 alloy in the different conditions considered. Tensile tests were performed at three different rates revealing almost no sensitivity to the rate of deformation. A slight sensitivity to the rate of deformation is apparent only for the base metal. The tensile results are summarized in Table 2. Three tensile tests for each condition were carried out at room temperature and the average values are listed herein. It can be seen that the stress levels of the base metal are higher in comparison to the FSWed alloy. The yield strength (Y.S.) and ultimate tensile strength (UTS) of the base metal are 56 and 17%, respectively, higher than those in the FSWed aluminum 7075 alloy. The decrease of stress levels can be attributed to the dissolution of the very fine hardening precipitates during FSW processing at 430 °C (Ref 30, 34). An adverse effect of FSW processing on the elongation of aluminum 7075 alloy is seen. The ST**AC**AA aluminum 7075 alloy specimen demonstrates inferior tensile properties as compared to that of the FSWed and base metal counterparts. The reason for such a severe deterioration in tensile properties of the ST**AC**AA aluminum 7075 alloy specimen can be rationalized by the formation of the large PFZs in the vicinity of GBs. It is well known that deformation can be localized in these zones being characterized by the absence of fine, strengthening precipitates. Eventually, these zones are prone to crack nucleation (Ref 26, 35). For the case of ST**WQ**AA aluminum 7075 alloy specimen, PWHT is able to recover the initial strength of the FSWed specimen by increasing Y.S. and UTS by about 49 and 11%, respectively. Mechanical strength improvement of welded specimen via PWHT is imputed to the reprecipitation of the precipitates previously dissolved during the welding process (Ref 17, 36). However, the ST**WQ**AA aluminum 7075 alloy specimen shows lower ductility as compared to base metal and the FSWed alloy. The poor ductility of this specimen might be attributed to the pronounced inhomogeneity in the microstructure, i.e., the presence of the very large grains induced by AGG (Fig. 4e). Therefore, deformation is strongly localized in the NZ, where the large grains are only present. Even an adequate distribution of precipitates is not sufficient to fully counterbalance this issue.

Strength values of the investigated specimens can also be traced by hardness measurements. Moreover, the hardness values provide for detailed information on the local strength of the alloy in its different conditions. Therefore, microhardness (HV 0.1) mappings were conducted on the aluminum 7075 alloy in different conditions (Fig. 7). The hardness value of the base metal was determined to be 193 HV. It can be seen that FSW processing degraded hardness of this alloy in both NZ and HAZ, whereas the remaining parts of the specimen retained at hardness values as high as in the base metal (Fig. 7a). Besides, hardness

Journal : **JMEP_11665**	Dispatch : **3-8-2019**	Pages : **11**
Article Number : **4252**	☐ LE ☑ CP	☐ TYPESET ☑ DISK

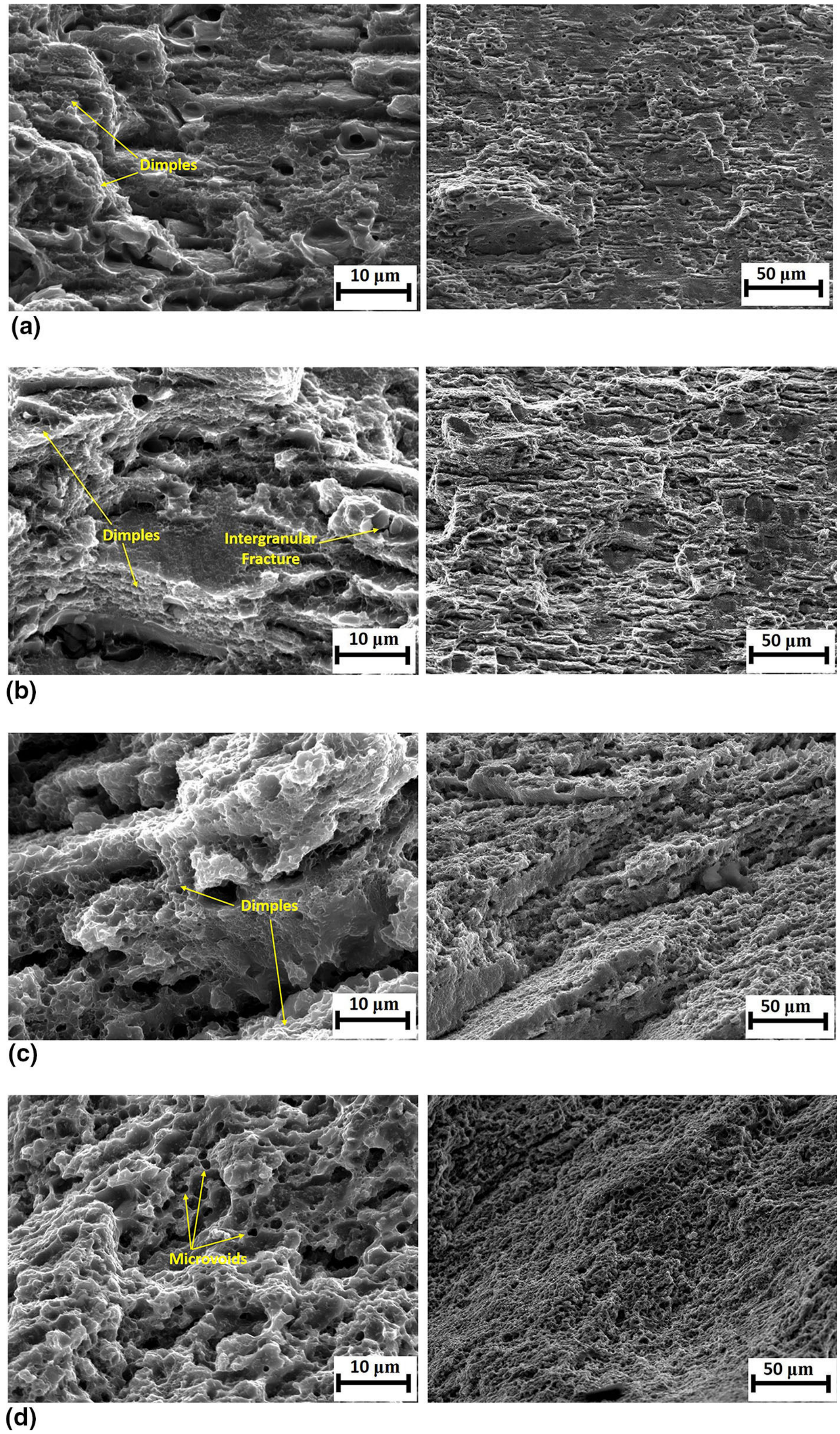

Fig. 8 Tensile fracture surfaces of (a) base metal (7075-T6 aluminum alloy), and (b) FSWed, (c) ST**AC**AA and (d) ST**WQ**AA aluminum 7075 alloy tested with a crosshead speed of 0.8 mm/min (The pictures on the left and right show high and low magnification, respectively)

values of the ST**AC**AA specimen remarkably decrease in comparison to both base metal and FSWed conditions (Fig. 7b). This can be rationalized based on the segregation of large precipitates along GBs and the formation of the PFZs as discussed earlier. These coarse-segregated precipitates consume the alloying elements needed for precipitation, and as a result, the minimized fraction of precipitates evolving within the subsequent aging step does not provide for efficient hardening of the material (Ref 37, 38). The hardness values of the ST**WQ**AA specimen are in the range of 180-197 HV clearly highlighting

Journal : **JMEP_11665** Dispatch : **3-8-2019** Pages : **11**
Article Number : **4252** ☐ LE ☑ CP ☐ TYPESET ☑ DISK

the positive impact of this PWHT on the overall material strength (Fig. 7c). The higher rate of cooling provides for a higher degree of supersaturation and, thus, allows for subsequent homogeneous precipitation during the second aging step (Ref 21, 23, 39). The microhardness results are in good agreement with the tensile properties of the specimens. The mechanical properties introduced above imply that precipitation hardening is more influential on strengthening of the aluminum 7075 alloy as the grain refinement achieved by FSW.

3.3 Fractography

To characterize the failure mechanisms of the aluminum 7075 alloy in different conditions, the fracture surfaces were analyzed. Representative fracture surfaces are shown in Fig. 8. Clearly, fracture morphologies of specimens upon the various processing histories are different. The fracture surface of the base metal is characterized by a mixture of both cleavage and dimple-like facets (as highlighted by arrows, Fig. 8a). This type of fracture morphology can be classified as transgranular fracture. Such kind of fracture behavior is associated with a much higher ductility as compared to intergranular fracture (Ref 40). The ST**AC**AA and ST**WQ**AA specimens both failed in the NZ. Cracking of the FSWed specimen occurred in the thermomechanically affected zone. The fracture surface of the FSWed specimen can be characterized by the presence of both dimples and intergranular facets (as highlighted by arrows, Fig. 8b). For this condition, transgranular fracture features are seen at a higher proportion than those related to intergranular fracture, i.e., features stemming from localized failure induced by the second phases on the GBs (Ref 17). The fracture surface of the ST**AC**AA specimen reveals different fracture morphology (Fig. 8c). As discussed earlier, the ST**AC**AA specimen contains large PFZs, which are characterized by lower strength and higher ductility as compared to the grain interiors. Therefore, the fracture seen in Fig. 8(c) might be ascribed to the localization of deformation in direct vicinity of the GB, promoted by the existence of second phase particles on the GBs eventually resulting in crack nucleation and propagation alongside these grain boundaries (Ref 29, 41, 42). Decohesion of second phases in GBs was reported to be one of the main reasons for the occurrence of the fracture in aluminum alloys (Ref 43, 44). The fracture analysis of the ST**AC**AA specimen is in good agreement with the observed brittle mechanical behavior of this condition. The fracture surface of the ST**WQ**AA specimen indicates the existence of microvoids on the exposed grain surface (as highlighted by arrows, Fig. 8d). However, the fracture surface indicates that the nature of fracture of the ST**WQ**AA specimen is not as brittle as that of the ST**AC**AA one. It is expected that in the ST**WQ**AA specimen due to the AGG induced heterogeneity of the microstructure deformation and eventually failure is limited to a very localized region of the specimen instead of the complete gauge section as in case of the base material. In situ tests would be able to clearly resolve this issue, however, are out of the scope of the present work and, thus, will be subject of future studies.

4. Conclusion

The effect of postweld heat treatment (PWHT) on the mechanical properties and microstructural evolution of friction-stir-welded (FSWed) aluminum 7075 alloy was studied by characterizing tensile and microhardness properties and analyzing underlying microstructural features. The following conclusion can be made based on the results detailed:

(i) Grain refinement took place in the nugget zone (NZ) of the aluminum 7075 alloy processed via FSW. The average grain size in the NZ was measured to be 2 μm. Grain growth was observed during solution treatment of PWHT. Abnormal grain growth developed for the water quenched (ST**WQ**AA) specimen, while the grain growth ceased during the aging of the air-cooled (ST**AC**AA) specimen indicating the restriction of grain boundary motion via segregated precipitates along GBs.

(ii) EDS and the SEM analysis of specimens revealed that segregation of large precipitates along the grain boundaries occurred for the specimen having lower cooling rate after solution treatment of PWHT. Consequently, PFZs were formed in the direct vicinity of GBs.

(iii) The formation of PFZs lowered the strength, hardness, and ductility of aluminum 7075 alloy, attesting the adverse impacts of PFZs on the mechanical properties of this alloy. Higher cooling rate was found to be beneficial for recovering mechanical properties of the welded specimen. This PWHT is associated with reprecipitation of dissolved strengthening particles in the NZ during aging.

(iv) Studies of the fracture surfaces implied that the fracture mechanism in the base metal is dominated by cleavages and a few dimples, while the intergranular type was the main mechanism for tensile fracture of specimens undergoing FSW.

(v) In light of the microstructural observations, precipitation hardening has a stronger influence on the attainable strength of FSWed joint than grain refinement induced by FSW.

Acknowledgments

The authors gratefully acknowledge financial support from the Hessen State Ministry for Higher Education, Research and the Arts—Initiative for the Development of Scientific and Economic Excellence (LOEWE) for the Project *ALLEGRO* (Subprojects A2, A3 and B1).

References

1. C.M. Cepeda-Jiménez, J.M. García-Infanta, O.A. Ruano, and F. Carreño, Mechanical Properties at Room Temperature of an Al-Zn-Mg-Cu Alloy Processed by Equal Channel Angular Pressing, *J. Alloys Compd.*, 2011, **509**(35), p 8649–8656. https://doi.org/10.1016/J.JALLCOM.2011.06.070
2. X.-M. Li and M.J. Starink, *Effect of Compositional Variations on Characteristics of Coarse Intermetallic Particles in Overaged 7000 Aluminium Alloys*, Taylor & Francis, Routledge, 2013, https://doi.org/10.1179/026708301101509449
3. R. Jayaganthan, H.-G. Brokmeier, B. Schwebke, and S.K. Panigrahi, Microstructure and Texture Evolution in Cryorolled Al 7075 Alloy, *J. Alloys Compd.*, 2010, **496**(1–2), p 183–188. https://doi.org/10.1016/J.JALLCOM.2010.02.111
4. K. Shojaei, S.V. Sajadifar, and G.G. Yapici, On the Mechanical Behavior of Cold Deformed Aluminum 7075 Alloy at Elevated Temperatures, *Mater. Sci. Eng., A*, 2016, **670**, p 81–89. https://doi.org/10.1016/j.msea.2016.05.113

Journal : **JMEP_11665** Dispatch : **3-8-2019** Pages : **11**
Article Number : **4252** ☐ LE ☑ CP ☐ TYPESET ☑ DISK

5. M. Prapas, N. Jennarong, and P. Woraphot, Effect of Post-Weld Heat Treatment on Microstructure and Mechanical Properties of Friction Stir Welded SSM7075 Aluminium Alloy, *J. Wuhan Univ. Technol. Sci. Ed.*, 2017, **32**(6), p 1420–1425. https://doi.org/10.1007/s11595-017-1763-y
6. P. Cavaliere and A. Squillace, High Temperature Deformation of Friction Stir Processed 7075 Aluminium Alloy, *Mater. Charact.*, 2005, **55**(2), p 136–142. https://doi.org/10.1016/J.MATCHAR.2005.04.007
7. P. Sivaraj, D. Kanagarajan, and V. Balasubramanian, Effect of Post Weld Heat Treatment on Tensile Properties and Microstructure Characteristics of Friction Stir Welded Armour Grade AA7075-T651 Aluminium Alloy, *Def. Technol.*, 2014, **10**(1), p 1–8. https://doi.org/10.1016/J.DT.2014.01.004
8. Y. Motohashi, T. Sakuma, A. Goloborodko, T. Ito, and G. Itoh, Grain Refinement Process in Commercial 7075-T6 Aluminum Alloy under Friction Stir Welding and Superplasticity, *Materwiss. Werksttech.*, 2008, **39**(4–5), p 275–278. https://doi.org/10.1002/mawe.200800288
9. A.H. Feng, D.L. Chen, and Z.Y. Ma, Microstructure and Cyclic Deformation Behavior of a Friction-Stir-Welded 7075 Al Alloy, *Metall. Mater. Trans. A*, 2010, **41**(4), p 957–971. https://doi.org/10.1007/s11661-009-0152-3
10. C.B. Fuller, M.W. Mahoney, M. Calabrese, and L. Micona, Evolution of Microstructure and Mechanical Properties in Naturally Aged 7050 and 7075 Al Friction Stir Welds, *Mater. Sci. Eng., A*, 2010, **527**(9), p 2233–2240. https://doi.org/10.1016/J.MSEA.2009.11.057
11. C.J. Dawes, W.M. Thomas, E.D. Nicholas, J.C. Needham, M.G. Murch, and P. Temple Smith, "Frictionstir Butt Welding" 1991
12. C. Genevois, A. Deschamps, A. Denquin, and B. Doisneau-cottignies, Quantitative Investigation of Precipitation and Mechanical Behaviour for AA2024 Friction Stir Welds, *Acta Mater.*, 2005, **53**(8), p 2447–2458. https://doi.org/10.1016/J.ACTAMAT.2005.02.007
13. A. Tamadon, D. Pons, K. Sued, D. Clucas, A. Tamadon, D.J. Pons, K. Sued, and D. Clucas, Thermomechanical Grain Refinement in AA6082-T6 Thin Plates under Bobbin Friction Stir Welding, *Metals (Basel)*, 2018, **8**(6), p 375. https://doi.org/10.3390/met8060375
14. K. Hockauf, M.F.-X. Wagner, T. Halle, T. Niendorf, M. Hockauf, and T. Lampke, Influence of Precipitates on Low-Cycle Fatigue and Crack Growth Behavior in an Ultrafine-Grained Aluminum Alloy, *Acta Mater.*, 2014, **80**, p 250–263. https://doi.org/10.1016/J.ACTAMAT.2014.07.061
15. Y. Lang, G. Zhou, L. Hou, J. Zhang, and L. Zhuang, Significantly Enhanced the Ductility of the Fine-Grained Al-Zn-Mg-Cu Alloy by Strain-Induced Precipitation, *Mater. Des.*, 2015, **88**, p 625–631. https://doi.org/10.1016/J.MATDES.2015.09.023
16. W. Yang, H. Ding, Y. Mu, J. Li, and W. Zhang, Achieving High Strength and Ductility in Double-Sided Friction Stir Processing 7050-T7451 Aluminum Alloy, *Mater. Sci. Eng., A*, 2017, **707**, p 193–198. https://doi.org/10.1016/J.MSEA.2017.09.028
17. P.V. Kumar, G.M. Reddy, and K.S. Rao, Microstructure, Mechanical and Corrosion Behavior of High Strength AA7075 Aluminium Alloy Friction Stir Welds: Effect of Post Weld Heat Treatment, *Def. Technol.*, 2015, **11**(4), p 362–369. https://doi.org/10.1016/J.DT.2015.04.003
18. A.A. Chegeni, P. Kapranos, A. Azadi Chegeni, and P. Kapranos, A Microstructural Evaluation of Friction Stir Welded 7075 Aluminum Rolled Plate Heat Treated to the Semi-Solid State, *Metals (Basel)*, 2018, **8**(1), p 41. https://doi.org/10.3390/met8010041
19. D.A. Tanner and J.S. Robinson, Effect of Precipitation during Quenching on the Mechanical Properties of the Aluminium Alloy 7010 in the W-Temper, *J. Mater. Process. Technol.*, 2004, **153–154**, p 998–1004. https://doi.org/10.1016/J.JMATPROTEC.2004.04.226
20. S. Liu, Q. Li, H. Lin, L. Sun, T. Long, L. Ye, and Y. Deng, Effect of Quench-Induced Precipitation on Microstructure and Mechanical Properties of 7085 Aluminum Alloy, *Mater. Des.*, 2017, **132**, p 119–128. https://doi.org/10.1016/J.MATDES.2017.06.054
21. H. Li, J. Liu, W. Yu, H. Zhao, and D. Li, Microstructure Evolution of Al-Zn-Mg-Cu Alloy during Non-Linear Cooling Process, *Trans. Nonferrous Met. Soc. China*, 2016, **26**(5), p 1191–1200. https://doi.org/10.1016/S1003-6326(16)64250-4
22. Y. Zhang, B. Milkereit, O. Kessler, C. Schick, and P.A. Rometsch, Development of Continuous Cooling Precipitation Diagrams for Aluminium Alloys AA7150 and AA7020, *J. Alloys Compd.*, 2014, **584**, p 581–589. https://doi.org/10.1016/J.JALLCOM.2013.09.014
23. S.T. Lim, S.J. Yun, and S.W. Nam, Improved Quench Sensitivity in Modified Aluminum Alloy 7175 for Thick Forging Applications, *Mater. Sci. Eng., A*, 2004, **371**(1–2), p 82–90. https://doi.org/10.1016/S0921-5093(03)00653-1
24. T.R. McNelley, S. Swaminathan, and J.Q. Su, Recrystallization Mechanisms during Friction Stir Welding/Processing of Aluminum Alloys, *Scr. Mater.*, 2008, **58**(5), p 349–354. https://doi.org/10.1016/J.SCRIPTAMAT.2007.09.064
25. M.A. Safarkhanian, M. Goodarzi, and S.M.A. Boutorabi, Effect of Abnormal Grain Growth on Tensile Strength of Al-Cu-Mg Alloy Friction Stir Welded Joints, *J. Mater. Sci.*, 2009, **44**(20), p 5452–5458. https://doi.org/10.1007/s10853-009-3735-x
26. H. Aydın, A. Bayram, and İ. Durgun, An Investigation on Microstructure and Mechanical Properties of Post-Weld Heat-Treated Friction Stir Welds in Aluminum Alloy 2024-W, *Proc. Inst. Mech. Eng. Part C J. Mech. Eng. Sci.*, 2013, **227**(4), p 649–662. https://doi.org/10.1177/0954406212452479
27. F.J. Humphreys, M. Hatherly, F.J. Humphreys, and M. Hatherly, Chapter 5: The Mobility and Migration of Boundaries. *Recrystallization and Related Annealing Phenomena*, 2004, p 121–167
28. H. Gleiter, The Mechanism of Grain Boundary Migration, *Acta Metall.*, 1969, **17**(5), p 565–573. https://doi.org/10.1016/0001-6160(69)90115-1
29. M.W. Mahoney, C.G. Rhodes, J.G. Flintoff, W.H. Bingel, and R.A. Spurling, Properties of Friction-Stir-Welded 7075 T651 Aluminum, *Metall. Mater. Trans. A*, 1998, **29**(7), p 1955–1964. https://doi.org/10.1007/s11661-998-0021-5
30. M. Reimann, J. Goebel, and J.F. dos Santos, Microstructure and Mechanical Properties of Keyhole Repair Welds in AA 7075-T651 Using Refill Friction Stir Spot Welding, *Mater. Des.*, 2017, **132**, p 283–294. https://doi.org/10.1016/J.MATDES.2017.07.013
31. M.J. Starink, Reduced Fracturing of Intermetallic Particles during Crack Propagation in Age Hardening Al-Based Alloys Due to PFZs, *Mater. Sci. Eng., A*, 2005, **390**(1–2), p 260–264. https://doi.org/10.1016/J.MSEA.2004.09.053
32. T.S. Srivatsan, D. Lanning, and K.K. Soni, Microstructure, Tensile Properties and Fracture Behaviour of an Al-Cu-Mg Alloy 2124, *J. Mater. Sci.*, 1993, **28**(12), p 3205–3213. https://doi.org/10.1007/BF00354237
33. C.G. Rhodes, M.W. Mahoney, W.H. Bingel, R.A. Spurling, and C.C. Bampton, Effects of Friction Stir Welding on Microstructure of 7075 Aluminum, *Scr. Mater.*, 1997, **36**(1), p 69–75. https://doi.org/10.1016/S1359-6462(96)00344-2
34. D.J. Lloyd and M.C. Chaturvedi, A Calorimetric Study of Aluminium Alloy AA-7075, *J. Mater. Sci.*, 1982, **17**(6), p 1819–1824. https://doi.org/10.1007/BF00540811
35. Y. Liu, D.M. Jiang, and W.J. Li, The Effect of Multistage Ageing on Microstructure and Mechanical Properties of 7050 Alloy, *J. Alloys Compd.*, 2016, **671**, p 408–418. https://doi.org/10.1016/J.JALLCOM.2016.01.266
36. G. Chu, L. Sun, C. Lin, and Y. Lin, Effect of Local Post Weld Heat Treatment on Tensile Properties in Friction Stir Welded 2219-O Al Alloy, *J. Mater. Eng. Perform.*, 2017, **26**(11), p 5425–5431. https://doi.org/10.1007/s11665-017-2998-7
37. J.W. Evancho and J.T. Staley, Kinetics of Precipitation in Aluminum Alloys during Continuous Cooling. *Metall. Trans.* n.d., **5**(1), p 43, https://doi.org/10.1007/bf02642924
38. J.T. Staley, Quench Factor Analysis of Aluminium Alloys, *Mater. Sci. Technol.*, 1987, **3**(11), p 923–935. https://doi.org/10.1179/mst.1987.3.11.923
39. M. Tiryakioğlu and R.T. Shuey, Quench Sensitivity of an Al-7 Pct Si-0.6 Pct Mg Alloy: Characterization and Modeling, *Metall. Mater. Trans. B*, 2007, **38**(4), p 575–582. https://doi.org/10.1007/s11663-007-9027-4
40. M.F. Ashby, Mechanisms of Deformation and Fracture, *Adv. Appl. Mech.*, 1983, **23**, p 117–177. https://doi.org/10.1016/S0065-2156(08)70243-6
41. A.K. Vasudévan and R.D. Doherty, Grain Boundary Ductile Fracture in Precipitation Hardened Aluminum Alloys, *Acta Metall.*, 1987, **35**(6), p 1193–1219. https://doi.org/10.1016/0001-6160(87)90001-0
42. M.-H. Ku, F.-Y. Hung, T.-S. Lui, and L.-H. Chen, Embrittlement Mechanism on Tensile Fracture of 7075 Al Alloy with Friction Stir Process (FSP), *Mater. Trans.*, 2011, **52**(1), p 112–117. https://doi.org/10.2320/matertrans.M2010315

Journal : **JMEP_11665**	Dispatch : **3-8-2019**	Pages : **11**
	☐ LE	☐ TYPESET
Article Number : **4252**	☑ CP	☑ DISK

43. L. Jiang, J.K. Li, P.M. Cheng, G. Liu, R.H. Wang, B.A. Chen, J.Y. Zhang, J. Sun, M.X. Yang, and G. Yang, Microalloying Ultrafine Grained Al Alloys with Enhanced Ductility, *Sci. Rep.*, 2015, **4**(1), p 3605. https://doi.org/10.1038/srep03605
44. T. Pardoen, D. Dumont, A. Deschamps, and Y. Brechet, Grain Boundary versus Transgranular Ductile Failure, *J. Mech. Phys. Solids*, 2003, **51**(4), p 637–665. https://doi.org/10.1016/S0022-5096(02)00102-3

Publisher's Note Springer Nature remains neutral with regard to jurisdictional claims in published maps and institutional affiliations.

Autorenversion von: Sajadifar, S.V., Moeini, G., Scharifi, E. et al. On the Effect of Quenching on Postweld Heat Treatment of Friction-Stir-Welded Aluminum 7075 Alloy. J. of Materi Eng and Perform 28, 5255–5265 (2019). https://doi.org/10.1007/s11665-019-04252-3

Journal : **JMEP_11665**	Dispatch : **3-8-2019**	Pages : **11**
	☐ LE	☐ TYPESET
Article Number : **4252**	☑ CP	☑ DISK